

Thawed Gaussian wave packet dynamics: a critical assessment of three propagation schemes

Ilya G. Ryabinkin,^{1, a)} Rami Gherib,¹ and Scott N. Genin¹

OTI Lumionics Inc., 3415 American Drive Unit 1,
Mississauga, Ontario L4V 1T4, Canada

(Dated: 25 July 2024)

We assessed three schemes for propagating a variable-width (thawed) Gaussian wave packet moving under the influence of Morse or double-well potentials with parameters that are chemically representative. The most rigorous scheme is based on the time-dependent variational principle (TDVP); it leads to realistic behaviour of the center and width of a wave packet in all investigated regimes. Two other approximate schemes, Heller’s and the extended semiclassical ones, demonstrate various aberrations. Heller’s scheme does not properly account for various zero-point energy-related effects, is unable to predict tunneling, and more importantly, exhibits completely nonphysical unbound width oscillations. The extended semiclassical scheme, which was developed to address some of the shortcomings of the Heller counterpart, demonstrates another unphysical behaviour: self-trapping of a trajectory in both Morse and double-well potentials. We conclude that only the TDVP-based scheme is suitable for problem-free dynamical simulations. This, however, raises the question of how to utilize it efficiently in high-dimensional systems.

I. INTRODUCTION

An essential part of theoretical modelling of novel fluorescent or phosphorescent materials for the display industry is simulation of their vibrationally resolved (vibronic) optical spectra. They are naturally accessible *via* the Fourier transform of a dipole-dipole autocorrelation function $C(t)$,^{1–4}

$$C(t) = \langle \Psi(0) | \Psi(t) \rangle \quad (1)$$

where $\Psi(0) = \mu_{fi}\chi_i$, is a product of nuclear wave function of the initial state χ_i and a transition dipole moment function μ_{fi} associated with an $i \rightarrow f$ electronic transition,

$$\Psi(t) = \exp(-i\hat{H}_f t)\Psi(0) \quad (2)$$

is a time-dependent wave function that evolves under the action of a nuclear Hamiltonian \hat{H}_f . Thus, the problem is reduced to exact or approximate quantum evolution of some initial wave function.

In the past decades, several exact methods for solving the time-dependent Schrödinger equation (TDSE) have been developed: the split-operator method,^{5–9} the Chebyshev polynomial expansion method,^{10,11} multiconfiguration time-dependent Hartree (MCTDH),^{12,13} and variational multi-configurational Gaussian (vMCG)¹⁴ methods, to name a few. However, exact methods in general scale exponentially with the number of quantum degrees of freedom (DOFs) and, are thus unsuitable for molecules of the size of typical light emitters.

Vibronic spectra simulations, on the other hand, rarely require accurate long-time dynamics. As a result, *approximate* quantum dynamics methods with better computational scaling and hence applicable to larger systems received a lot of attention. One of the oldest yet

still very popular approach uses a single Gaussian wave packet to represent a nuclear wave function.^{15–36} The exact time evolution of a wave function is replaced by time evolution of Gaussian parameters; to derive the corresponding equations of motion (EOMs) different guiding rules may be applied. In this paper we consider the three most popular schemes for the Gaussian propagation: Heller’s scheme, also known as the local harmonic approximation (LHA),¹⁵ its correction—the extended semiclassical dynamics,^{21,28} and the full, most rigorous scheme based on the time-dependent variational principle (TDVP),^{37,38} which was independently derived by many authors^{18–21,23,24,27,29,33,39–44} though not all of them recognized that they used one of the equivalent formulations of TDVP.⁴⁵

An early assessment of both approximate schemes—Heller’s and the extended semiclassical ones—was made by Pattanayak and Schieve²¹ who considered the dynamics of a Gaussian wave packet placed atop of a barrier at $x = 0$ of a quartic potential, $V(x) = ax^4 - bx^2 + c$, with $a, b > 0$. They observed that the wave packet spread without bounds, which was clearly unphysical. Qualitative differences between Heller’s and the extended semiclassical schemes were reported in a study of a tunneling escape from a cubic potential $V(x) = x^2/2 - cx^3$, $c = 1/10$.²⁸ The Heller trajectory remained trapped, while the semiclassical one escaped through a barrier. Heather and Metiu⁴¹ compared the Heller scheme with their “minimum error method”, which was a TDVP-based scheme in disguise, and noticed that the former showed substantially larger deviations from the exact quantum result than the latter, even in the low-energy regime when oscillations took place near the minimum of the potential. They speculated that the observed errors could be attributed to disregarding the Heisenberg’s principle and poor description of the zero-point energy (ZPE) in the Heller approximation. Several additional issues were documented by the same authors in Ref. 46. A failure of Heller’s scheme in sim-

^{a)}Electronic mail: ilya.ryabinkin@otilumionics.com

ulations of liquid argon was noted in Ref. 40. However, in a study of collinear ICN photodissociation,²⁰ Heller’s scheme demonstrated reasonable agreement with more accurate TDVP-based Gaussian dynamics. Heller’s scheme coupled with on-the-fly calculations of *ab initio* molecular energies, gradients, and Hessians was recently employed in simulations of optical and photoelectron spectra of polyatomic molecules and the reported outcomes were encouraging.^{34,47,48} The full TDVP-based scheme—to the best of our knowledge—was used only twice in simulations of realistic systems: solid and liquid argon with the Lennard-Jones potential fitted by a linear combination of Gaussians,⁴⁰ and liquid water employing analytically parameterised intra- and intermolecular potentials.²⁷ In the latter work, the observed differences in simulated IR and Raman spectra between the TDVP-based scheme and purely classical simulations as well as better agreement with experimental spectra for the former were attributed to proper description of essential quantum effects. Surprisingly, although multiple successful applications and a few points of failures were reported, a systematic comparative assessment of all three Gaussian propagation schemes is still missing in the literature.

In this study, our primary goal is to create a consistent picture of the successes and failures of the Gaussian propagation schemes. To this end, we study their performance for one-dimensional (1D) model anharmonic potentials, “quantum potentials” for short, which allows us to decouple a question of the quality of employed potentials from consequences of dynamical approximation. Our quantum potentials are also amenable for extensive analytical treatment, and we complement our numerical results with analytical considerations. Although it was entirely possible, we refrained from the comparison to the exact quantum results as in realistic molecular applications the exact quantum solution will not be available. Instead, we focus on the analysis of internal consistency of the resulting dynamics.

Our analysis relies on a unique mapping between 1D *quantum* dynamics of a thawed Gaussian wave packet and 2D *classical* dynamics of a fictitious particle of the same mass moving under the influence of an *extended potential* $U(q, w)$, where q and w are the position of the center and the width of the corresponding Gaussian.^{18,19,21} As we show, U compactly encodes some features that are commonly referred to as “quantum”, for example, ZPE,^{49–57} so that our analysis extends beyond purely dynamical perspective.

The paper is organized as follows. First, we formulate the EOMs for all three schemes in a common form using the aforementioned mapping. Next, we introduce our model potentials—the Morse and the double-well ones—that are parametrized to represent realistic physical systems. We analyse a static picture and consider several dynamical regimes, such as a small-amplitude motion near a minimum, barrier tunneling/penetration, and large amplitude motion. We assess not only spectroscopic, but also mechanical properties and we attempt to identify

all cases when the approximate schemes fail and rationalize why. What is beyond the scope of our study is the vibrational mode coupling due to anharmonicity as well as Dushinsky⁴ rotations — both require genuine multi-dimensional potentials. However, many shortcomings of approximate schemes are evident even in 1D systems.

II. THEORY

A. Thawed Gaussian dynamics as classical dynamics in extended phase space

An N -dimensional Gaussian wave packet (N being the number of quantum DOFs in a problem) is customarily parameterized as^{15,40}

$$\psi(\mathbf{x}, t) = \exp \left\{ \frac{i}{\hbar} [(\mathbf{x} - \mathbf{q}_t)^T A_t (\mathbf{x} - \mathbf{q}_t) + \mathbf{p}_t \cdot (\mathbf{x} - \mathbf{q}_t) + \gamma_t] \right\}, \quad (3)$$

where \mathbf{q}_t and \mathbf{p}_t are time-dependent coordinates and momenta of a center of the Gaussian in coordinate and momentum spaces, respectively, A_t is an $N \times N$ complex symmetric time-dependent matrix, and γ_t is a complex scalar. In what follows, the case of $N = 1$, in which vectors and matrices in Eq. (3) become scalars, is exclusively considered. For brevity, of all parameters are assumed to be time dependent, and the subscript t is suppressed.

Parametrization of a Gaussian wave packet as in Eq. (3) is not physically transparent. While p and q are quantum-mechanical averages of the position and momentum operators, respectively,

$$\langle \hat{x} \rangle = q, \quad (4)$$

$$\langle \hat{p} \rangle = p, \quad (5)$$

the physical meaning of A is obscured by its complex-valued nature. One can separate real and imaginary parts of A and parametrize them as

$$A = \frac{u}{2w} + i \frac{\hbar}{4w^2}, \quad (6)$$

so that the one-dimensional Gaussian assumes the form¹⁸

$$\psi(x, t) = \exp \left\{ -\frac{1}{4w^2} \left(1 - 2iw \frac{u}{\hbar} \right) (x - q)^2 + \frac{i}{\hbar} p (x - q) + \frac{i}{\hbar} \lambda \right\}, \quad (7)$$

and

$$\frac{\int |\psi(x, t)|^2 (x - q)^2 dx}{\int |\psi(x, t)|^2 dx} = w^2, \quad (8)$$

giving w the meaning of the width of a wave packet. $\lambda = \Re\{\gamma\}$ is a real parameter, whereas the imaginary part of γ can be absorbed into the norm \mathcal{N} ,

$$\mathcal{N}^2 = \langle \psi | \psi \rangle = \sqrt{2\pi} w. \quad (9)$$

Time evolution of the parameters p , q , w , u , and λ can be derived in the most general way using the TDVP.^{37,38} The resulting EOMs are¹⁸

$$\dot{q} = \{q, \mathcal{H}\} = \frac{p}{m}, \quad (10a)$$

$$\dot{p} = \{p, \mathcal{H}\} = -\frac{\partial U}{\partial q}, \quad (10b)$$

$$\dot{w} = \{w, \mathcal{H}\} = \frac{u}{m}, \quad (11a)$$

$$\dot{u} = \{u, \mathcal{H}\} = -\frac{\partial U}{\partial w}, \quad (11b)$$

where dots symbolize the full time derivative, $\{\cdot, \cdot\}$ are Poisson brackets and \mathcal{H} is a classical Hamilton function in a *four*-dimensional phase space of canonically conjugated variables (p, q) and (u, w) defined by the quantum Hamiltonian

$$\hat{H} = -\frac{\hbar^2}{2m} \frac{d^2}{dx^2} + V(x) \quad (12)$$

as

$$\mathcal{H}(q, p, w, u) = \mathcal{N}^{-2} \langle \psi | \hat{H} | \psi \rangle = \frac{p^2}{2m} + \frac{u^2}{2m} + U(q, w), \quad (13)$$

$$U(q, w) = \frac{\hbar^2}{8mw^2} + \frac{1}{\sqrt{2\pi}} \int_{-\infty}^{\infty} V(wx + q) e^{-x^2/2} dx. \quad (14)$$

Thus, quantum dynamics of one-dimensional Gaussian is exactly represented by classical dynamics of a particle in a phase space whose dimensionality is twice as large as that of the parent quantum model. As was mentioned above, w is a width of the packet and u is a momentum canonically conjugated to it.

The last equation that is relevant to computations of optical spectra is the EOM for the position-independent phase of a wave packet, λ . It reads²¹

$$\dot{\lambda} = \frac{\dot{w}u - \dot{u}w}{2} + p\dot{q} - E, \quad (15)$$

with

$$E = \mathcal{H}|_{\text{at the trajectory}}. \quad (16)$$

B. Representations of $U(q, w)$ and approximate dynamical schemes

The downside of a classical view on the thawed Gaussian dynamics is that U requires evaluation of a parametric integral in Eq. (14). $U(q, w)$ is an even function of w ; additionally, if V is analytic, one can write²¹

$$\frac{1}{\sqrt{2\pi}} \int_{-\infty}^{\infty} V(wx + q) e^{-x^2/2} dx = V(q) + \sum_{n=1}^{\infty} V^{(2n)}(q) \frac{w^{2n}}{2^n n!}. \quad (17)$$

Numerical evaluation of $U(q, w)$ *via* integration or series (17) summation is computationally intensive unless U can be found in a closed form.^{22,23,27}

In order to employ realistic, possibly *ab initio* potentials V , simplified means to compute U are thus highly desirable. The lowest-order approximations of U that follow from Eq. (17) are:

$$U^0(q, w) = \frac{\hbar^2}{8mw^2} + V(q), \quad (18)$$

$$U^1(q, w) = \frac{\hbar^2}{8mw^2} + V(q) + \frac{w^2}{2} V''(q). \quad (19)$$

$U^0(q)$ is separable, and dynamics of (p, q) and (u, w) guided by $U = U^0$ is fully decoupled: a particle of a mass m with a momentum p and a position q feels a classical force $-V'(q)$, while the width w grows infinitely under a purely repulsive force $\hbar^2/4mw^3$. The latter behaviour is consistent with a Gaussian wave packet moving and spreading on a potential with vanishing second- and higher-order derivatives (flat potentials) but is less relevant to molecules. At the next order, the potential $U^1(q, w)$ can be evaluated in a closed form for potentials V that are at most quadratic in x ,

$$U^{\text{LHA}}(q, w) = \frac{\hbar^2}{8mw^2} + V(q) + \frac{kw^2}{2}, \quad (20)$$

where $k = V''(q) = \text{const}$ is a (force) constant. For such potentials the EOMs for the pair (p, q) are still purely classical as $-\partial U^{\text{LHA}}/\partial q = -V'(q)$ because the derivative of a constant term $kw^2/2$ vanishes. The EOMs for the (u, w) pair can be converted into a second-order equation,

$$m\ddot{w} = \frac{\hbar^2}{4mw^3} - kw, \quad (21)$$

and integrated analytically (see, for example, Ref. 18) to give harmonic oscillations of w around the initial value w_0 with an amplitude that vanishes when

$$w_0 = (\hbar^2/4mk)^{1/4}, \quad (22)$$

which is a width of a Gaussian *coherent state*.^{39,58}

The assumption that the quantum potential V can be replaced by its quadratic approximation centered at q —the local harmonic approximation (LHA)—was originally considered by Heller¹⁵. The resulting EOMs, purely classical for the (p, q) pair and given by Eqs. (11a–11b) with $U = U^1(q, w)$ for the pair (u, w) , are known as Heller's dynamics.^{15,21} It is exact for harmonic potentials, but Heller himself suggested to apply it to *anharmonic* potentials, for which $V''(q)$ is not constant. One inconsistency of this approach, which was pointed out by Pattanayak and Schieve²¹ (see also Ref. 28), is immediately clear: EOMs for pairs (p, q) and (u, w) employ potentials that differ by more than a constant if $V(q)$ is anharmonic. To restore consistency and use, for example, a common $U^1(q, w)$, one must write

$$\dot{p} = -\frac{\partial U^1}{\partial q} = -V'(q) - \frac{w^2}{2} V^{(3)}(q). \quad (23)$$

Thus-modified EOMs constitute the “extended semiclassical dynamics” in the terminology of Pattanayak and Schieve²¹. The presence of the third derivative of V as well as coupling between (p, q) and (u, w) pairs make the extended semiclassical dynamics computationally intensive.

The EOM for the phase λ is also modified. For both approximate schemes one must use

$$E = \frac{p^2}{2m} + \frac{u^2}{2m} + U^1(q, w) \quad (24)$$

in Eq. (16).²¹ Note that the semiclassical dynamics conserves E as defined by Eq. (24) while Heller’s dynamics conserves only classical energy $E_{\text{cl}} = \frac{p^2}{2m} + V(q)$. This is another inconsistency in the Heller approach.

III. SIMULATIONS SETUP

A. Model potentials

We employed two one-dimensional anharmonic potentials. The first is the Morse potential,⁵⁹

$$V_{\text{M}}(x) = D_e \left[1 - e^{-b(x-a)} \right]^2 - D_e, \quad (25)$$

which describes stretching of an O–H bond in certain types of clays.⁶⁰ The reduced mass of a particle associated with this type of motion is chosen to be a proton mass, $m \approx 1836 m_e$. Numerical values of the parameters D_e , a , and b are listed in Table I.

The second model potential is a double-well potential for the inversion motion in ammonia, NH_3 .⁶¹ It is a combination of a harmonic well and a Gaussian barrier at its center,

$$V_{\text{A}}(x) = \frac{1}{2} k x^2 + b e^{-c x^2}, \quad (26)$$

Numerical values of the parameters and the reduced mass m for the inversion motion are given in Table I.

TABLE I. Parameters of the model potentials.

Parameter	Value	
	atomic units	common units
<i>Morse potential, Eq. (25)</i>		
D_e	0.210 752	132.2491 kcal mol ⁻¹
a	1.785 79	0.9450 Å
b	1.154 40	2.1815 Å ⁻¹
m	1836.15	1.007 28 Da
<i>Ammonia double-well potential, Eq. (26)</i>		
k	0.075 98	11.83 × 10 ⁴ dyns/cm
b	0.056 84	2.478 × 10 ⁻¹² erg
c	1.3696	4.891 × 10 ¹⁶ cm ⁻²
m	4668	2.561 Da

B. Evaluation of the extended potential

The extended potential $U(q, w)$ can be found in a closed form for both model potentials, Eqs. (25) and (26), respectively:

$$U_{\text{M}}(u, w) = \frac{\hbar^2}{8mw^2} + D_e \left[e^{-2b(q-a-bw^2)} - 2e^{-b(q-a-bw^2/2)} \right], \quad (27)$$

$$U_{\text{A}}(u, w) = \frac{\hbar^2}{8mw^2} + \frac{1}{2} k (q^2 + w^2) + \frac{b}{\sqrt{z}} e^{-c q^2 / z}, \quad (28)$$

where $z = 1 + 2cw^2$.

Application of the thawed Gaussian dynamics together with *ab initio* potentials requires numerical schemes for computing U . We implemented two such schemes. The first one is applying an n -point Gauss-Hermite quadrature⁶² to the Gaussian integral in Eq. (14),

$$\int_{-\infty}^{\infty} V(wx + q) e^{-x^2/2} dx \approx \sqrt{2} \sum_{i=1}^n g_i V(\sqrt{2}wx_i + q), \quad (29)$$

where $\{x_i\}_{i=1}^n$ and $\{g_i\}_{i=1}^n$ are the corresponding nodes and weights. The second scheme is direct summation of a power series, Eq. (17). It is straightforward when analytical derivatives of $V(x)$ are known, but computationally less convenient because high-order derivatives are rarely available *ab initio*. However, this scheme allowed us to cross-check all the formulas and also implement evaluation of $U^1(q, w)$, Eq. (19).

C. Equations of motion

The TDVP-based dynamical scheme follows Eqs. (10) and (11) with the full $U(q, w)$ calculated by Eqs. (27) and (28) for Morse and ammonia double-well potentials, respectively. Phase evolution is determined by Eqs. (15) and (16).

In Heller’s scheme EOMs for the (p, q) pair are purely classical

$$\dot{q} = \frac{p}{m}, \quad (30a)$$

$$\dot{p} = -V'(q), \quad (30b)$$

while the EOMs for the (u, w) pair are Eqs. (11a) and (11b) with $U \equiv U^1(q, w)$ given by Eq. (19).

The extended semiclassical scheme uses Eqs. (10) and (11) with $U = U^1(q, w)$. In both approximate schemes the phase is propagated by Eq. (15) with E evaluated by Eq. (24).

D. Software

All the potentials and dynamical models as well as auxiliary routines are implemented in Julia language⁶³

and available on GitHub.⁶⁴ The equations of motion are integrated using the explicit Runge–Kutta 5(4) method with the updated tableau of coefficients⁶⁵ available as `Tsit5` algorithm in the `DifferentialEquations.jl`⁶⁶ Julia package.

IV. RESULTS AND DISCUSSION

A. Convergence issues in approximations to the extended potential

In general, numerical evaluation of the extended potential either by integration or through summation of the Taylor series (see Sec. III B) becomes more challenging for larger w . Additionally, Taylor series summation poses a problem of convergence. Consider as an example the ammonia double-well model. The width variable w enters the exact expression for the extended potential $U_A(q, w)$, Eq. (28), as functions $z^{-\frac{1}{2}}$ and z^{-1} where $z = 1 + 2cw^2$. Taylor series of both functions converge only for $|2cw^2| < 1$ (equivalently, $|w| < \sqrt{\frac{1}{2c}}$), so is the Taylor expansion (17).

We report convergence of numerical approximations (denoted as \tilde{U}_A) to $U_A(q, w)$, which employed the 10-point Gauss-Hermite quadrature and the Taylor series with 10 terms in Table II. We show the mean and the maximum of an absolute deviation $|U_A(q, w) - \tilde{U}_A(q, w)|$ for the range of q from -2.0 to $2.0 a_0$ (discretized on an equidistant grid with 101 points) and a few selected values of w : 0.1 , 0.6 and $1.0 a_0$. For the smallest value of $w = 0.1 a_0$ both numerical schemes converge to high accuracy. For $w = 0.6 a_0$, which is close to the convergence radius $0.604 a_0$, the Taylor series demonstrates noticeable deviations from reference values; it also converges very slowly upon adding more terms. Finally, for $w = 1.0 a_0$ the Taylor series clearly diverge, while the Gauss-Hermite scheme is still reasonably accurate. Gaussian integration is applicable for larger values of w , but more points are needed for the same accuracy. Larger integration grids, however, makes multi-dimensional generalizations challenging, which may prompt researchers to consider Monte Carlo integration instead.

It must be emphasized that convergence issues are independent of representation: while they were demonstrated in parameterization (7), they impact *any* approximate schemes that exploit the series expansion in a variable related to the width.

B. Static limit

Consider for simplicity the Morse potential, which has only one (global) minimum. When the amplitude of oscillations vanishes⁶⁷, one obtains a static limit, in which

TABLE II. Convergence of numerical approximations \tilde{U}_A to the exact ammonia extended potential U_A .

Approximation	$ U_A(q, w) - \tilde{U}_A(q, w) , E_h$	
	mean	max
	$w = 0.1 a_0$	
Gauss–Hermite	2.9×10^{-17}	8.3×10^{-17}
Taylor	1.8×10^{-12}	5.3×10^{-12}
	$w = 0.6 a_0$	
Gauss–Hermite	3.2×10^{-7}	8.2×10^{-7}
Taylor	0.0021	0.0062
	$w = 1.0 a_0$	
Gauss–Hermite	8.8×10^{-5}	0.000 19
Taylor	0.53	1.5

all conjugate momenta are zero:

$$\dot{p} = 0, \quad (31)$$

$$\dot{u} = 0. \quad (32)$$

For the Heller, the extended semiclassical, and the TDVP-based schemes the condition (31) translates into

$$\frac{dV_M(x)}{dx} = 0, \quad (33)$$

$$\frac{\partial U_M^1}{\partial q} = 0, \quad (34)$$

$$\frac{\partial U_M}{\partial q} = 0, \quad (35)$$

respectively, where $U_M^1(q, w)$ is given by Eq. (19) with $V \equiv V_M$. Thus, in Heller’s scheme a wave packet is stationary at the minimum (usually referred to as r_e) of the quantum potential V_M , while for the other models stationary points are different. Analytical consideration is difficult for the full U_M , but is possible for U_M^1 . Solving Eq. (34) one obtains

$$e^{-b(q_{\min} - a)} = 1 - \frac{3w^2 b^2}{2 + 4w^2 b^2} \equiv \alpha < 1 \quad \forall w > 0, \quad (36)$$

which means $(q_{\min} - a) = -\ln(\alpha)/b > 0$, or $q_{\min} > a \equiv r_e$. We expect the same inequality holds for the full $U_M(q, w)$, at least if anharmonicity is not too strong. Turning to the numerical methods we located global minima of U_M and U_M^1 and found q_{\min} to be $1.8130 a_0$ and $1.8133 a_0$, respectively,—larger than that for the Morse potential, whose $q_{\min} = r_e \equiv a = 1.7858 a_0$ (see Table I and Fig. 1). Thus, Heller’s scheme predicts noticeable shorter equilibrium O–H distance than the TDVP-based or the extended semiclassical scheme. This result is in agreement with observations made in Ref. 27, where similar elongation was reported in simulations of liquid water.

Ranking of schemes changes if we consider how well the ground vibrational energy is approximated. The full TDVP-based scheme conforms with the (stationary) variational principle approaching the true energy from above. In the static limit, when Eqs. (31) and (32) hold, finding

the minimum of $U(q, w)$ is equivalent to minimization of the expectation value of the quantum Hamiltonian [see Eq. (13)] using a Gaussian as a wave-function *Ansatz*. The minimum of U_M lies 1909.4 cm^{-1} above the bottom of the Morse potential well, which is within 10 cm^{-1} from the true ground-state energy, 1899.45 cm^{-1} ; see Fig. 1. For the extended semiclassical scheme one should seek for a minimum of U_M^1 , which is located 1874.3 cm^{-1} above the bottom of the potential well. This scheme, therefore, underestimates the ground-state energy by approximately 25 cm^{-1} . Finally, for Heller’s scheme, while the *location* of the static wave packet can be found—in q variable it coincides with the minimum of V_M whereas for w it is given by the condition $\partial U_M^1/\partial w = 0$ —its energy cannot be unambiguously assigned. Measuring energy through U_M , or, equivalently as an expectation value of the quantum Hamiltonian on the static wave packet, one finds it equals to 1954.7 cm^{-1} . Measured as a value of U_M^1 at the location of the static wave packet, the energy equals to 1919.4 cm^{-1} , being approximately 20 cm^{-1} above the exact. This value ranks Heller’s scheme second in accuracy. This situation can be explained by partial error cancellation between approximations to the extended potential and the variational principle for Heller’s scheme. It must be admitted that discrepancies between schemes are small compared to the absolute energy of the ground state but they clearly demonstrate yet another ambiguity existing in Heller’s scheme.

For quantum potentials V with a unique minimum (*e.g.* V_M), the difference between it and that of U_M can be interpret as ZPE,⁵⁰ see Fig. 1. Even more, one can give a local, position-dependent definition of ZPE as follows. If we minimize $U_M(q, w)$ with respect to w at every q , then this quantity is larger than $V_M(q)$ near the minimum of V_M (the difference is positive), but *smaller* than $V_M(q)$ near dissociation (the difference is negative); see the dotted curve in Fig. 1. Therefore, the point-wise positivity of thus-defined ZPE is not guaranteed. As follows from Eq. (19) this takes place approximately when $V''(x) < 0$. However, this definition provides a simple explanation of tunneling: near the top of a barrier where $V''(x) < 0$, ZPE may act as a source of energy driving barrier penetration. We elaborate on that in Sec. IV D.

The dotted line in Fig. 1 depicts the minimal possible energy of a wave packet, which ascends from the minimum towards the dissociation infinitely slowly (adiabatically). One can call such a packet the *minimum uncertainty* wave packet, thus explaining the naming of the corresponding potential curve.

C. Dynamics in a small-amplitude regime

Let us again concentrate on the Morse potential. We simulate dynamics with the following initial conditions: the initial position $q_0 = 1.6 a_0$, the initial width $w_0 = 0.125 a_0$, all conjugated momenta p_0 and u_0 , as well as the initial value of the phase λ_0 , are zero. Thus, the

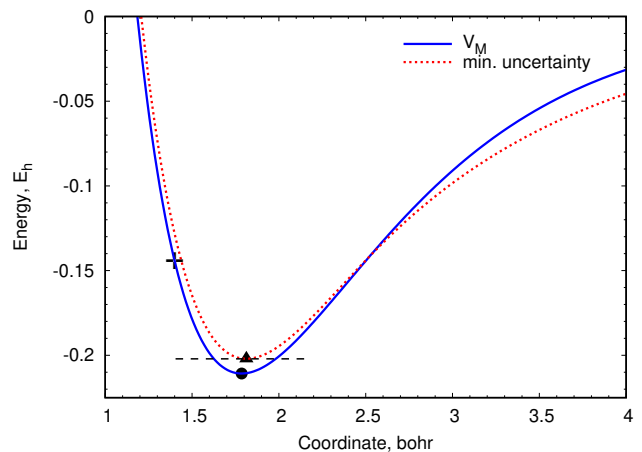


FIG. 1. Quantum Morse potential V_M (solid line) and the minimum uncertainty potential $\min_w U_M(q, w)$ (dotted line). A dashed horizontal line is a position of the ground vibrational level of V_M . A dot labels the (global) minimum of V_M whereas a triangle is a coordinate of the global minimum of $U_M(q, w)$. A black cross marks the initial position of a wave packet for the setup discussed in Sec. IV E.

wave packet is initially placed on a repulsive branch of the potential close to the minimum (see Fig. 1) and its starting width is close yet not exactly matches the coherent state width, Eq. (22), to induce small oscillations in both q and w directions.

Since the adaptive algorithm to integrate EOMs was used, the integration time step was variable, but the solution was interpolated on a regular time grid with a step size $dt = 4.03 \text{ au}$ (atomic units of time) using the default implementation available in `DifferentialEquations.jl`. The total propagation time corresponded to $n_t = 2^{14} = 16384$ time steps to provide reasonable spectral resolution. Absolute and relative accuracy requirements for integration were: `abstol = reltol = 1.0 × 10-8`.

1. Mechanical motion

Figure 2 shows oscillations of a linear momentum $p(t)$ of a wave packet. The most notable feature in Fig. 2 is a different amplitude of oscillations in the extended semiclassical scheme as compared to both the TDVP-based and Heller’s ones. We attribute these differences to exaggerated coupling between position and width in the extended semiclassical scheme that allows for faster energy exchange between these DOFs. However, a more important characteristic of dynamics is an oscillation period. Simple counting reveals that in the time span shown in Fig. 2 there are 13 oscillation periods for the TDVP-based scheme but 14 periods for Heller’s one. Therefore, the characteristic vibrational frequency in the latter is $1/13$ times higher than in former, which is substantial. It is known that the red-shift of the OH fundamental frequency is an important quantum effect in liquid water.²⁷ Hence, Heller’s scheme fails to properly account for this

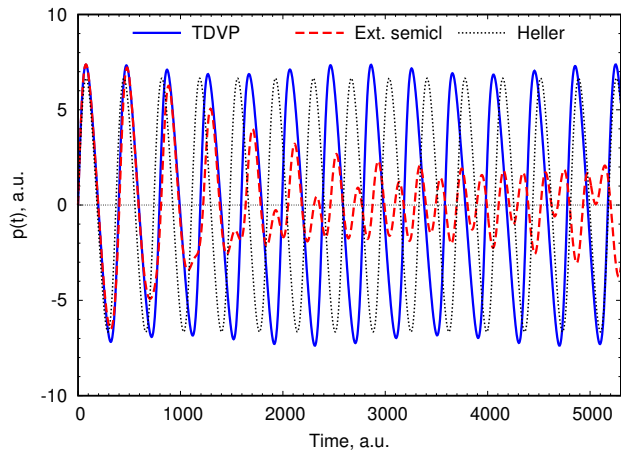


FIG. 2. Linear momentum dynamics for the small-amplitude motion in the Morse potential.

quantum anharmonic effect.

To our great surprise, we discovered a much more fundamental flaw of Heller’s scheme in describing the mechanical motion in this system, which is clearly visible in Fig. 3. Width oscillations remain finite in the TDVP-based and extended semiclassical schemes, but in Heller’s scheme grow linearly in time without bounds. As follows from Eqs. (30a) and (30b) the width dynamics in Heller’s scheme does not affect linear motion of a wave packet. On the contrary, the EOMs for the (u, w) pair, Eqs. (11a) and (11b) carry parametric dependence on the position variable q . Thus, the observed phenomenon can be considered as a form of a *parametric resonance*.

A natural question is whether this phenomenon is universal or specific to the Morse potential. We ran a small-amplitude dynamics for the ammonia potential; results are shown in Appendix . We observe very similar behaviour of the width for Heller’s dynamics: an unbound oscillatory growth of the amplitude albeit on a different time scale. Thus, the unbound growth of the width amplitude has nothing to do with natural spreading of a wave packet in regions where a potential has vanishing second- and higher-order derivatives (“flat regions”)—the ammonia potential is nowhere flat. The unbound growth does not exist for strictly quadratic potentials, but even minuscule anharmonicity causes it to manifest. Fundamentally, this phenomenon is due to the lack of back-reaction of the width dynamics onto position of a Gaussian wave packet. Re-establishing of this coupling, as was done in the extended semiclassical scheme is therefore crucial for curing this deficiency; otherwise, an evolving Gaussian wave packet must not be used to compute quantum-mechanical averages of any property. In light of this prediction, it is interesting to analyse (power) spectra predicted by the schemes.

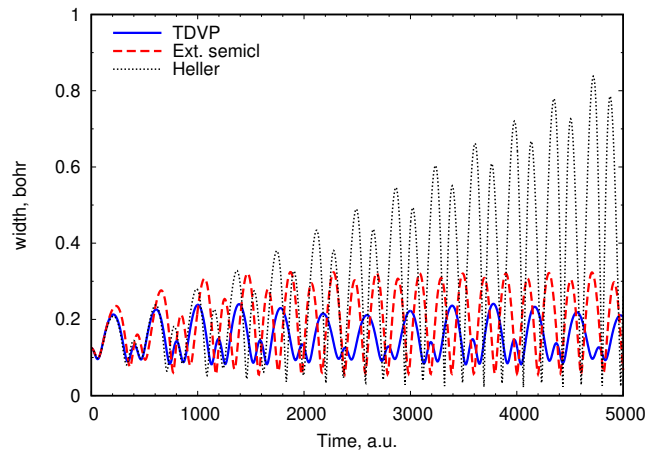


FIG. 3. Width dynamics for the small-amplitude motion in the Morse potential.

2. Spectra

We computed spectra via the Fourier transform of the autocorrelation function, Eq. (1), as

$$I(\omega) = \lim_{T \rightarrow \infty} \frac{1}{2\pi} \int_{-T}^T C(t) e^{i(\omega - E_0/\hbar)t} dt, \quad (37)$$

where E_0 is the origin of the energy scale, which is chosen to be the energy of the bottom of the Morse potential well in order to enable comparison of excitation energies with eigenenergies.

Numerically, the integral in Eq. (37) is evaluated from 0 to finite T using the fact that $C(-t) = C^*(t)$ (time reversibility) via the Fast Fourier transform and taking the real part of the result. Truncation at finite T , however, may introduce a jump discontinuity, unless the interval $[0; T)$ contains an integer multiple of an oscillation period. For such periodic signals the imaginary part of $I(\omega)$ vanishes and one could use either real or absolute parts. We carefully chosen the upper limit $T = t_0 + (n_t - 1)dt = 66\,023.49$ au (see Sec. IV C) to minimize the jump discontinuity⁶⁸. The absolute value $|I(\omega)|$ (in arbitrary units) along with the vibrational eigenlevels of the Morse potential (vertical black lines) are plotted in Fig. 4.

As evident from Fig. 4, the TDVP-based scheme shows peaks at energies that are very close to vibrational eigenenergies. Moreover, relative peak intensities are reproduced fairly well: expansion of the initial Gaussian over a set of bound-state Morse eigenfunctions gives relative weights 1:0.59:0.26:0.11, which are visually close to majors peaks heights in Fig. 4. On the other hand, the TDVP-based scheme also demonstrates (spurious) weak satellite peaks (*e.g.* one near 6000 cm^{-1}), which are probably caused by a resonance between position and width oscillations. Satellite peaks are more pronounced in the extended semiclassical scheme (see the inset in Fig. 4), but the positions

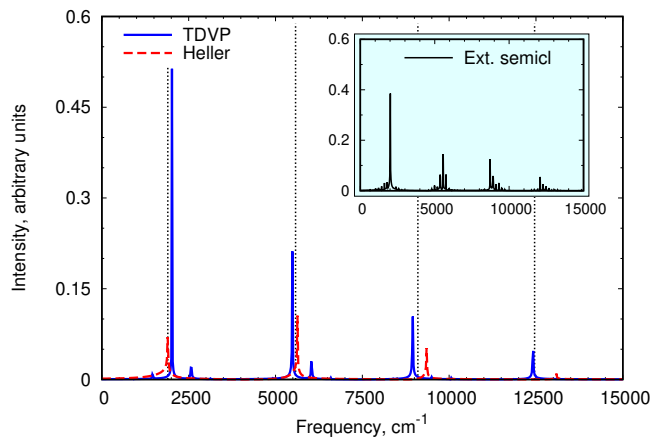


FIG. 4. Absorption spectra $|I(\omega)|$ computed by Eq. (37) (arbitrary units). Vertical black dotted lines are vibrational eigenlevels of the Morse potential.

and intensities of the major peaks are reasonably close to those given by the TDVP-based counterpart.

Despite the pathological *mechanical* behaviour discussed in Sec. IV C 1, the spectrum given by Heller’s scheme is surprisingly accurate. The ground- and the first excited-state peak positions are very close to the exact energies, only the second and higher peaks start to deviate. It appears, therefore, that the spurious large-amplitude width oscillations have little impact on the computed autocorrelation function and hence, the spectrum. We explain this by the observation that spectra are mainly determined by a short-time behaviour of the autocorrelation function $C(t)$, Eq. (1). In practice, it is usually damped to zero to account for the environmental effects, and the unbound growth of the width provides a somewhat strange mechanism to drive $C(t)$ to zero. On the other hand, the *width* of the spectral lines, which is inversely proportional to a natural lifetime of a wave packet, in this case has nothing to do with any environmental effects, and in fact is determined by the strength of anharmonicity of the parent quantum potential.

Spectral intensities are less satisfactorily reproduced by Heller’s scheme. For example, the most intensive (highest) peak is assigned to the first excited state, not the ground one. Nevertheless, in typical spectroscopic applications intensities are usually considered to be of lesser importance than peaks positions.

Overall, our findings partly explain why the flaws of Heller’s scheme went unnoticed in the majority of previous studies, which were mainly focused on spectroscopic applications. In one work,⁴⁸ however, rising amplitude of the semiclassical energy (24) in a course of dynamics was reported—see Fig. 3 there. Ultimately, this phenomenon is related to the pathological width dynamics.

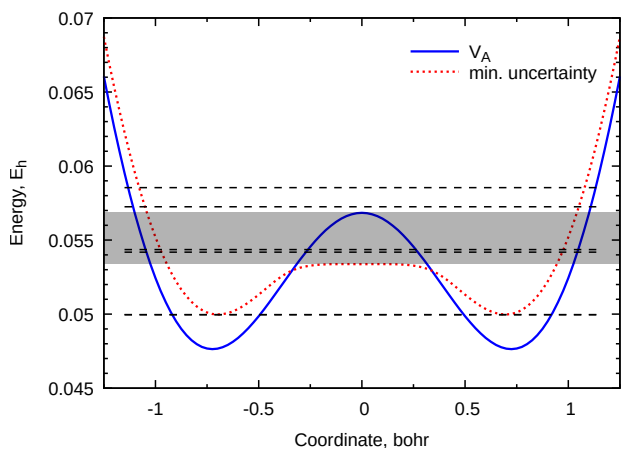


FIG. 5. Ammonia double-well potential V_A (solid line) and $\min_w U_A(q, w)$ (dotted line). Dashed horizontal lines denote vibrational levels of V_A . Note that the ground and the first excited state are almost degenerate and visually indiscernible. A shaded area is a region of energies in which tunneling of a wave packet is possible in the TDVP-based scheme.

D. Tunneling dynamics

Tunneling dynamics is modelled for the ammonia double-well potential shown in Fig. 5. As it was done for the Morse potential, we numerically computed the minimal uncertainty potential $\min_w U_A(q, w)$ shown as a red dotted line in Fig. 5. In a range of energies between its local maxima and the maximum of V_A near $q = 0$ (shaded area in Fig. 5) a wave packet can tunnel through a barrier in the TDVP-based scheme. We simulated the dynamics in the tunneling regime using the following initial conditions: initial position and width are $-1.0 a_0$ (the left well) and $0.15 a_0$, respectively, all the conjugate momenta and the initial phase are zero. The accuracy parameters for the time integration, `abstol` and `reltol`, were tightened to 1.0×10^{-12} . Trajectory data were interpolated on a regular time grid with a time step $dt = 4.03 \text{ au}$.

Time evolution of the coordinate of a center of a wave packet $q(t)$ is shown in Fig. 6. As anticipated, the wave packet tunnels through a barrier in the TDVP-based scheme while in Heller’s scheme it stays inside the left well. However, the most notable feature in Fig. 6 is the trapping of the semiclassical trajectory at the top of the barrier, $q = 0$. This unexpected result can be explained as follows. The effective potential in the extended semiclassical scheme $U_A^1(q, w)$, Eq. (19), contains a contribution that depends on the curvature of the potential $V_A''(q)$ at a position of a wave packet. Near $q = 0$ the curvature is *negative*, so both $V(q)$ and $V''(q)w^2/2$ terms have a shape of a curved-down parabola. If a wave packet passes this region slowly enough, these contributions drive the width of the packet to infinity and essentially remove the maximum at $q = 0$ turning it into a minimum. It must be noted that a very shallow parabolic well centered at $q = 0$ with the depth $\sim 2 \times 10^{-6} E_h$ exists for the minimum uncertainty potential $\min_w U_A(q, w)$ even for the exact U_A though this

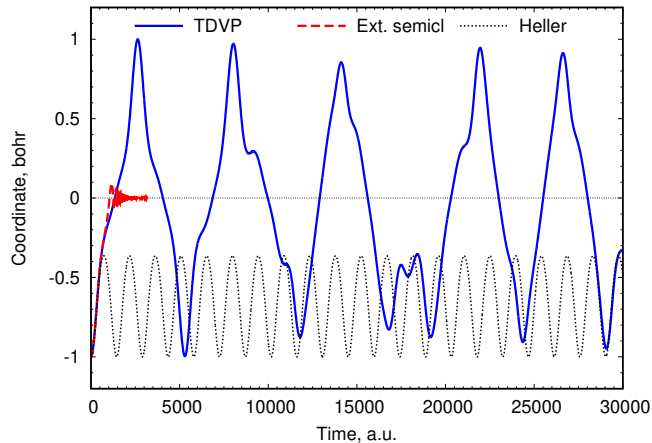


FIG. 6. Time evolution of the coordinate of a center of Gaussian wave packet $q(t)$ in the double-well ammonia potential; see Fig. 5.

region appears essentially flat in Fig. 5. Thus, the wave packet may be trapped in the TDVP-based scheme too, but this requires fine tuning of the initial parameters: the packet must be placed on the top of the barrier from the beginning, and its width must be carefully optimized. No divergence of the width to infinity is possible, so one may speculate that the TDVP-based scheme predicts some sort of quantum *resonance* in this case.

We validated our explanation by performing two tests. First, we verified that a sufficiently fast wave packet could avoid trapping. If the initial position is set to $q_0 = -1.6 a_0$, which corresponds to the initial energy well above the top of the barrier (see Fig. 5), then the center of a wave packet exhibits similar dynamics in all three schemes for at least 1.3×10^5 au. Second, a slow wave packet in the region of negative curvature can be realized near a classical turning point of the *Morse* potential in a region where $V_M''(q) < 0$. We consider this scenario in the next section.

E. Trapping of the extended semiclassical trajectory in the large-amplitude motion in the Morse potential well

We simulated large-amplitude dynamics for the Morse potential using the following initial parameters: the initial position and width are $1.4 a_0$ and $0.125 a_0$, respectively, all the conjugated momenta and the initial phase are zero. These initial conditions are labelled by a black cross in Fig. 1. The accuracy parameters for the time integration, `abstol` and `reltol`, were set to 1.0×10^{-12} , the time step dt for interpolation was, as before, 4.03 au.

As anticipated, the trajectory given by the extended semiclassical scheme, gets trapped after initially entering into the negative curvature region of V_M . Only when the initial energy is high enough and above the dissociation limit, (*e.g.* for $q_0 = 1.1 a_0$), the extended semiclassical dynamics avoids trapping. That is, the extended semiclassical dynamics beaks down near classical turning points in regions of negative curvature of the quantum potential.

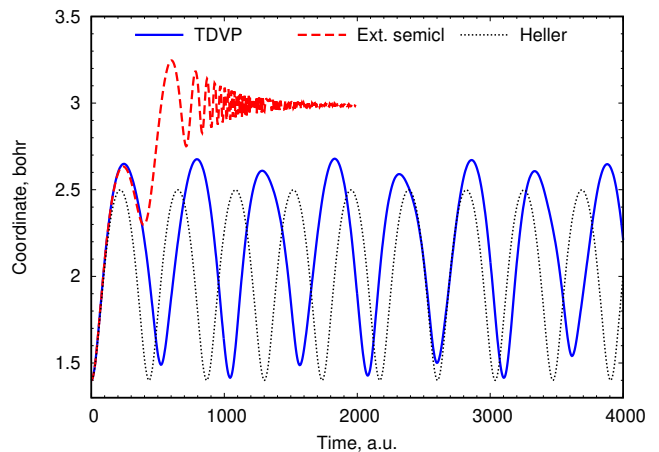


FIG. 7. Same as in Fig. 6 but for the Morse potential. The initial wave packet position is marked with a black cross in Fig. 1.

V. CONCLUSIONS

The main message of our work is that the TDVP-based propagation scheme is devoid of physical artefacts and only it should be used to simulate short- and intermediate-time quantum dynamics with anharmonic potentials. It is able to capture important quantum effects. It properly accounts for ZPE both in a static picture (see Sec. IV B) by distinguishing the (ro-)vibrational state-averaged equilibrium distance r_0 and r_e and providing $r_0 > r_e$,⁶⁹ and in dynamics by predicting the red shift of a frequency of mechanical oscillations (see Sec. IV C 1). It provides accurate spectral lines positions and intensities if the initial energy is not too high; see Fig. 4. Finally, it describes quantum tunneling *via* the mechanism that can be dubbed as ZPE-assisted: in regions of negative potential curvature energy “stored” in the width variable can be used by a wave packet to overcome a barrier; see Sec. IV D. The missing quantum effects are related to inability of a single Gaussian to bifurcate and (self)-interfere. Additionally, experimental initial conditions are better represented by a thermal density matrix rather than a pure wave function. However, a satisfactory density-based TDVP formalism was only recently developed⁷⁰ on the basis of the matrix Schrödinger equation for open systems;⁷¹ to the best of our knowledge it is not yet been applied to the thawed Gaussian dynamics.

The oldest and by far the most widely used Heller scheme gained its popularity due to relative algorithmic simplicity and compatibility with on-the-fly calculations of *ab initio* energies, gradients, and Hessian (force constant) matrices—there is no need to fit a potential energy surface beforehand. Additionally, the scheme provides very easy access to vibronic spectra via the directly simulated autocorrelation function $C(t)$, Eq. (1). We found, however, that it failed to provide a better physical picture than that given by classical mechanics. Because the equations of motion for this scheme, Eqs. (30a) and

(30b), are purely classical, a Gaussian wave packet visits exactly the same regions of a (p, q) phase space as a classical trajectory does. Heller’s scheme does not properly account for quantum anharmonic effects. Namely, it does not distinguish between r_0 and r_e in the static limit and cannot predict a red shift of a frequency of mechanical oscillations, see Secs. IV B and IV C 1. Moreover, due to the lack of coupling between position and width, Heller’s dynamics is unable to describe tunneling *via* the ZPE-assisted mechanism. The most serious drawback of Heller’s scheme is unbound oscillatory growth of the width in a process that resembles a parametric resonance as demonstrated in Sec. IV C 1. This phenomenon has nothing to do with proper wave packet spreading on flat potentials. It does not exist for strictly quadratic potentials and appears only for anharmonic ones with non-vanishing higher derivatives. In view of all these fundamental issues, it might be not clear though, why absorption spectra predicted by Heller’s scheme are often so surprisingly accurate. We explain this as follows. In many cases spectra are predominantly determined by a short-time behaviour of the autocorrelation function $C(t)$. In practice, $C(t)$ is usually damped to zero in account for environmental effects, and the unbound growth of the width provides a somewhat strange mechanism to drive $C(t)$ to zero. On the other hand, the width of spectral lines, which is inversely proportional to a natural lifetime of a wave packet, in this case has nothing to do with any environmental effects, and in fact is determined by the strength of anharmonicity of the parent quantum potential. Summarising, we strongly advise researchers against any use of a Gaussian wave packet parametrized by results of Heller’s dynamics in computations of expectation values of position- and especially width-dependent operators for times that are greater than a few width oscillation periods—see, for example, Fig. 3.

The extended semiclassical scheme was devised to improve upon the Heller counterpart. While it indeed corrects the dynamics in the static limit and for small-amplitude motions, it is susceptible to completely unphysical trapping of a trajectory in regions of negative potential curvature when a wave packet moves slowly. That means that neither tunneling (see Sec. IV D), nor large-amplitude motion (see Sec. IV E) can be described by this scheme without modifications. One needs to go to higher-order terms in Eq. (17) to reach a derivative that is positive in the region where a wave packet evolves, but in this case the problem of convergence of the Taylor series illustrated in Sec. IV A may render this approach invalid, not even mentioning the fact that higher than third derivatives are virtually unavailable in electronic structure packages.

While the current manuscript was in preparation, we became aware of recent works^{72–74} that have a strong overlap with our work. Our analysis is founded on the properties of the extended potential U and complements these works substantially identifying flaws that have never been previously documented.

Reiterating, we strongly believe that the TDVP-based scheme is best suited for reliable simulations of approximate quantum dynamics. The main challenge, however, is in combining it with *ab initio* potentials, preferably computed on the fly. As we shown in Sec. IV A, despite its poor scaling, a grid-based scheme may be exploited for low-dimensional problems. For high-dimensional systems a prospective solution could be to fit *ab initio* potentials locally using non-parametric regression techniques. The nuclear configurations used for the fitting could be sampled by initially identifying the nuclear subspace most relevant for dynamics. Indeed, as shown in our follow-up paper,⁷⁵ not all nuclear DOFs are always dynamically relevant, and many can be neglected in fitting. Sampling along a small number of dynamically relevant DOFs might mitigate the curse of dimensionality and ultimately allow the TDVP-based scheme to be utilised on industrially relevant molecules.

ACKNOWLEDGMENTS

I.G.R. is grateful to Profs. P. Brumer and A.F. Izmaylov from the University of Toronto for bringing attention to the thawed Gaussian dynamics back in 2017.

Appendix: Width dynamics in the ammonia potential

We initiate small-amplitude dynamics near the left minimum of the ammonia potential (see Fig. 5) using the following initial conditions: the initial position $q_0 = -0.9 a_0$, the initial width $w_0 = 0.15 a_0$, and $p_0 = u_0 = \lambda_0 = 0$. The width dynamics is shown in Fig. 8. Contrary to the full TDVP and the extended semiclassical models which predict oscillations with finite amplitudes, Heller’s model exhibits linear growth of the amplitude similar to that shown in Fig. 3. This clearly demonstrates that this phenomenon is not merely caused by the existence of flat regions in the potential (as in the Morse potential), but is a more general drawback of Heller’s scheme.

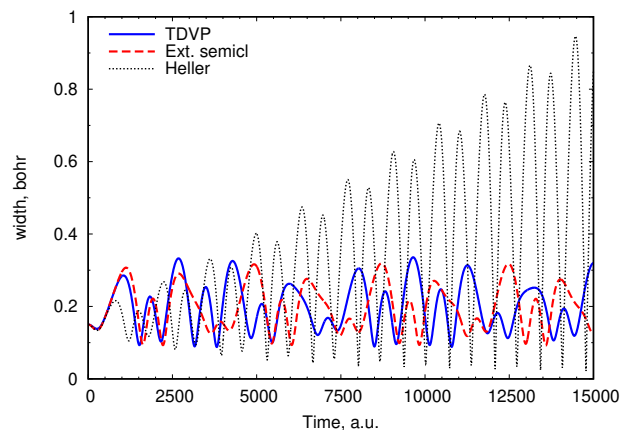


FIG. 8. Width dynamics for the ammonia model potential.

- ¹E. J. Heller, *J. Chem. Phys.* **68**, 2066 (1978).
- ²E. J. Heller, *Acc. Chem. Res.* **14**, 368 (1981).
- ³S. Mukamel, *J. Chem. Phys.* **77**, 173 (1982).
- ⁴A. Baiardi, J. Bloino, and V. Barone, *J. Chem. Theory Comput.* **9**, 4097 (2013), PMID: 26592403.
- ⁵J. A. Fleck, J. R. Morris, and M. D. Feit, *Appl. Phys.* **10**, 129 (1976).
- ⁶M. D. Feit, J. A. Fleck, and A. Steiger, *J. Comput. Phys.* **47**, 412 (1982).
- ⁷M. D. Feit and J. A. Fleck, *J. Chem. Phys.* **78**, 301 (1983).
- ⁸M. D. Feit and J. A. Fleck, *J. Chem. Phys.* **80**, 2578 (1984).
- ⁹A. D. Bandrauk and H. Shen, *Can. J. Chem.* **70**, 555 (1992).
- ¹⁰H. Tal-Ezer and R. Kosloff, *J. Chem. Phys.* **81**, 3967 (1984).
- ¹¹N. Balakrishnan, C. Kalyanaraman, and N. Sathyamurthy, *Phys. Rep.* **280**, 79 (1997).
- ¹²H.-D. Meyer, U. Manthe, and L. Cederbaum, *Chem. Phys. Lett.* **165**, 73 (1990).
- ¹³H. Wang and M. Thoss, *J. Chem. Phys.* **119**, 1289 (2003).
- ¹⁴G. Richings, I. Polyak, K. Spinlove, G. Worth, I. Burghardt, and B. Lasorne, *Int. Rev. Phys. Chem.* **34**, 269 (2015).
- ¹⁵E. J. Heller, *J. Chem. Phys.* **62**, 1544 (1975).
- ¹⁶S.-Y. Lee and E. J. Heller, *J. Chem. Phys.* **76**, 3035 (1982).
- ¹⁷M. F. Herman and E. Kluk, *Chem. Phys.* **91**, 27 (1984).
- ¹⁸F. Arickx, J. Broeckhove, E. Kesteloot, L. Lathouwers, and P. V. Leuven, *Chem. Phys. Lett.* **128**, 310 (1986).
- ¹⁹K. Singer and W. Smith, *Mol. Phys.* **57**, 761 (1986).
- ²⁰R. D. Coalson and M. Karplus, *J. Chem. Phys.* **93**, 3919 (1990).
- ²¹A. K. Pattanayak and W. C. Schieve, *Phys. Rev. E* **50**, 3601 (1994).
- ²²K. Ando, *Chem. Phys. Lett.* **376**, 532 (2003).
- ²³K. Ando, *J. Chem. Phys.* **121**, 7136 (2004).
- ²⁴G. A. Worth, M. A. Robb, and I. Burghardt, *Faraday Discuss.* **127**, 307 (2004).
- ²⁵E. Faou and C. Lubich, *Comput. Vis. Sci.* **9**, 45 (2006).
- ²⁶I. Burghardt, K. Giri, and G. A. Worth, *J. Chem. Phys.* **129**, 174104 (2008).
- ²⁷K. Hyeon-Deuk and K. Ando, *J. Chem. Phys.* **131**, 064501 (2009).
- ²⁸T. Ohsawa and M. Leok, *J. Phys. A: Math. Theor.* **46**, 405201 (2013).
- ²⁹D. Skouteris and V. Barone, *J. Chem. Phys.* **140**, 244104 (2014).
- ³⁰D. J. Coughtrie and D. P. Tew, *J. Chem. Phys.* **143**, 044102 (2015).
- ³¹B. Gu and S. Garashchuk, *J. Phys. Chem. A* **120**, 3023 (2016).
- ³²M. Vacher, M. J. Bearpark, and M. A. Robb, *Theor. Chem. Acc.* **135** (2016), 10.1007/s00214-016-1937-2.
- ³³L. Joubert-Doriol, J. Sivasubramaniam, I. G. Ryabinkin, and A. F. Izmaylov, *J. Phys. Chem. Lett.* **8**, 452 (2017).
- ³⁴A. Patoz, T. Begušić, and J. Vaníček, *J. Phys. Chem. Lett.* **9**, 2367 (2018).
- ³⁵S. Han, D. Xie, and H. Guo, *J. Chem. Theory Comput.* **14**, 5527 (2018).
- ³⁶I. Polyak, G. W. Richings, S. Habershon, and P. J. Knowles, *J. Chem. Phys.* **150**, 041101 (2019).
- ³⁷P. Kramer and M. Saraceno, eds., *Geometry of the Time-Dependent Variational Principle in Quantum Mechanics*, 1st ed., Lecture Notes in Physics, Vol. 140 (Springer Berlin, Heidelberg, 1981).
- ³⁸K.-K. Kan, *Phys. Rev. A* **24**, 2831 (1981).
- ³⁹A. K. Rajagopal and J. T. Marshall, *Phys. Rev. A* **26**, 2977 (1982).
- ⁴⁰N. Corbin and K. Singer, *Mol. Phys.* **46**, 671 (1982).
- ⁴¹R. Heather and H. Metiu, *Chem. Phys. Lett.* **118**, 558 (1985).
- ⁴²S.-I. Sawada, R. Heather, B. Jackson, and H. Metiu, *J. Chem. Phys.* **83**, 3009 (1985).
- ⁴³J. Grad, Y. J. Yan, A. Haque, and S. Mukamel, *J. Chem. Phys.* **86**, 3441 (1987).
- ⁴⁴I. Burghardt, H. D. Meyer, and L. S. Cederbaum, *J. Chem. Phys.* **111**, 2927 (1999).
- ⁴⁵J. Broeckhove, L. Lathouwers, E. Kesteloot, and P. V. Leuven, *Chem. Phys. Lett.* **149**, 547 (1988).
- ⁴⁶R. Heather and H. Metiu, *J. Chem. Phys.* **84**, 3250 (1986).
- ⁴⁷M. Wehrle, M. Šulc, and J. Vaníček, *J. Chem. Phys.* **140**, 244114 (2014).
- ⁴⁸M. Wehrle, S. Oberli, and J. Vaníček, *J. Phys. Chem. A* **119**, 5685 (2015).
- ⁴⁹W. H. Miller, W. L. Hase, and C. L. Darling, *J. Chem. Phys.* **91**, 2863 (1989).
- ⁵⁰R. Alimi, A. García-Vela, and R. B. Gerber, *J. Chem. Phys.* **96**, 2034 (1992).
- ⁵¹G. H. Peslherbe and W. L. Hase, *J. Chem. Phys.* **100**, 1179 (1994).
- ⁵²M. Ben-Nun and R. D. Levine, *J. Chem. Phys.* **101**, 8768 (1994).
- ⁵³T. D. Sewell, D. L. Thompson, J. D. Gezelter, and W. H. Miller, *Chem. Phys. Lett.* **193**, 512 (1992).
- ⁵⁴K. F. Lim and D. A. McCormack, *J. Chem. Phys.* **102**, 1705 (1995).
- ⁵⁵Y. Guo, D. L. Thompson, and T. D. Sewell, *J. Chem. Phys.* **104**, 576 (1996).
- ⁵⁶S. Habershon and D. E. Manolopoulos, *J. Chem. Phys.* **131**, 244518 (2009).
- ⁵⁷G. Czako, A. L. Kaledin, and J. M. Bowman, *J. Chem. Phys.* **132**, 164103 (2010).
- ⁵⁸A. Perelomov, *Generalized Coherent States and Their Applications*, Theoretical and Mathematical Physics (Springer Science & Business Media, 2012).
- ⁵⁹P. M. Morse, *Phys. Rev.* **34**, 57 (1929).
- ⁶⁰J. A. Greathouse, J. S. Durkin, J. P. Larentzos, and R. T. Cygan, *J. Chem. Phys.* **130**, 134713 (2009).
- ⁶¹J. D. Swalen and J. A. Ibers, *J. Chem. Phys.* **36**, 1914 (1962).
- ⁶²A. Townsend, T. Trogdon, and S. Olver, *IMA J. Numer. Anal.* **36**, 337 (2015), arXiv:1410.5286 [math.NA].
- ⁶³J. Bezanson, A. Edelman, S. Karpinski, and V. B. Shah, *SIAM Review* **59**, 65 (2017).
- ⁶⁴I. G. Ryabinkin, R. Gherib, and S. N. Genin, “Replication package for ‘Thawed Gaussian wave packet dynamics: a critical assessment of three propagation scheme’,” online (2024).
- ⁶⁵C. Tsitouras, *Comput. Math. with Appl.* **62**, 770 (2011).
- ⁶⁶C. Rackauckas and Q. Nie, *J. Open Res. Softw.* **5** (2017).
- ⁶⁷Vanishing amplitudes may be a result of statistical averaging of multiple trajectories with random initial conditions, so the static limit is important when dynamical simulations are used to compute thermodynamic properties.
- ⁶⁸Another popular approach to minimize truncation effects is damping of the autocorrelation function by multiplying it by $\exp(-\kappa t)$ with $\kappa > 0$ to ensure $C(T) \rightarrow 0$ along with all its derivatives. This corresponds to a convolution of the spectrum with a Lorentzian line shape function with the width $\sim 1/\kappa$. We do not apply this technique here.
- ⁶⁹T. Hirano, U. Nagashima, and M. Baba, *J. Mol. Struct.* **1229**, 128637 (2021).
- ⁷⁰D. Picconi and I. Burghardt, *J. Chem. Phys.* **150**, 224106 (2019).
- ⁷¹L. Joubert-Doriol, I. G. Ryabinkin, and A. F. Izmaylov, *J. Chem. Phys.* **141**, 234112 (2014).
- ⁷²J. J. L. Vaníček, *J. Chem. Phys.* **159**, 014114 (2023).
- ⁷³R. Moghaddasi Fereidani and J. J. L. Vaníček, *J. Chem. Phys.* **159**, 094114 (2023).
- ⁷⁴R. Moghaddasi Fereidani and J. J. L. Vaníček, *J. Chem. Phys.* **160**, 044113 (2024).
- ⁷⁵R. Gherib, I. G. Ryabinkin, and S. N. Genin, “Thawed Gaussian wavepacket dynamics with Δ -machine learned potentials,” online (2024), arXiv:2405.00193 [physics.chem-ph].